A THESIS SUBMITTED TO
THE GRADUATE SCHOOL OF NATURAL AND APPLIED SCIENCES
OF ÇANKIRI KARATEKİN UNIVERSITY

INVESTIGATION OF ANTIBACTERIAL PROPERTIES OF DOPED ZnO THIN FILMS PREPARED BY SILAR TECHNIQUE

IN PARTIAL FULFILLMENT OF THE REQUIREMENTS
FOR
THE DEGREE OF MASTER OF SCIENCE
IN
PHYSICS

BY

MOHAMED ABDULHUSEIN MOHSIN AL-SUDANI

ÇANKIRI

2023

INVESTIGATION OF ANTIBACTERIAL PROPERTIES OF DOPED ZnO THIN FILMS PREPARED BY SILAR TECHNIQUE

By Mohamed Abdulhusein Mohsin AL-SUDANI

February 2023

We certify that we have read this thesis and that in our opinion it is fully adequate, in scope and in quality, as a thesis for the degree of Master of Science

Advisor **:** Asst. Prof. Dr. İlker KARA

Examining Committee Members:

Chairman **:** Prof. Dr. Özcan YALÇINKAYA
Department of Chemistry
Gazi University

Member **:** Assoc. Prof. Dr. Olcay GENÇYILMAZ
Department of Material and Material Processing Technologies
Çankırı Karatekin University

Member **:** Asst. Prof. Dr. İlker KARA
Department of Medical Services and Techniques
Çankırı Karatekin University

Approved for the Graduate School of Natural and Applied Sciences

Prof. Dr. İbrahim ÇİFTÇİ
Director of Graduate School

I hereby declare that all information in this document has been obtained and presented in accordance with academic rules and ethical conduct. I also declare that, as required by these rules and conduct, I have fully cited and referenced all material and results that are not original to this work.

Mohamed Abdulhusein Mohsin AL-SUDANI

ABSTRACT

INVESTIGATION OF ANTIBACTERIAL PROPERTIES OF DOPED ZnO THIN FILMS PREPARED BY SILAR TECHNIQUE

Mohamed Abdulhusein Mohsin AL-SUDANI

Master of Science in Physics

Advisor: Asst. Prof. Dr. İlker KARA

February 2023

Metal oxides show semiconductor properties with their structures consisting of two or more elements. It is especially preferred due to its electrical conductivity, optical properties, chemical stability, biological non-toxicity and low cost. ZnO is one of the most preferred metal oxides in technological applications today. In this thesis study, undoped ZnO thin films and ZnO thin films with different additives were grown on ITO substrate by using the SILAR method. Thin films have been grown by the SILAR method in 40 cycles and then samples have been annealed at 300 °C. Structural, surface morphological, antibacterial and bacterial adhesion and survival properties of undoped, Ni-doped and Al-doped ZnO/ITO thin films were investigated. SEM/EDS method was used for surface morphology, agar diffusion test was used for bacterial analysis, and also organism count method was used for bacterial adhesion and survival. Surface morphologies of undoped, Ni-doped and Al-doped thin films showed differences in SEM analysis. Moreover, it has been determined that spherical, clustered and layer-shaped structures are formed. The antibacterial activities of the agar diffusion test were examined and it was seen that it did not show antibacterial activity to the produced samples. In bacterial adhesion and survival organism count, the highest adhesion rate was observed in the Ni-doped thin film.

2023, 49 pages

Keywords: SILAR method, Zinc oxide, Antibacterial activity

ÖZET

SILAR YÖNTEMİYLE HAZIRLANAN KATKILI ZnO İNCE FİLMLERİN ANTİBAKTERİYEL ÖZELLİKLERİNİN İNCELENMESİ

Mohamed Abdulhusein Mohsin AL-SUDANI
Fizik, Yüksek Lisans
Tez Danışmanı: Dr. Öğr. Üyesi İlker KARA
Şubat 2023

Metal oksitler, iki ya da daha fazla elementten oluşan yapılarıyla yarıiletken özelliği göstermektedir. Özellikle elektriksel iletkenliği, optik özellikleri, kimyasal stabilitesi, biyolojik olarak toksik olmaması ve düşük maliyeti nedeniyle tercih edilmektedir. Günümüzde ZnO, teknolojik uygulamalarda en sıklıkla tercih edilen metal oksitlerdendir. Bu tez çalışmasında SILAR yöntemi kullanılarak katkısız ve farklı katkılı ZnO ince filmleri ITO alltaş üzerine büyütülmüştür. İnce filmler, SILAR yöntemiyle 40 döngüde üretildikten sonra, 300 °C sıcaklıkta tavlanandı. Katkısız, Ni ve Al katkılı ZnO/ITO ince filmlerin yapısal, yüzeysel morfolojik, antibakteriyel, bakteriyel yapışma ve hayatta kalma özellikleri araştırılmıştır. Yüzey morfolojisi SEM/EDS yöntemiyle, bakteri analizlerinde ise agar difüzyon testi, bakteriyel yapışma ve hayatta kalma organizma sayımı yöntemiyle yapılmıştır. SEM analizlerinden katkısız, Ni ve Al katkılı ince filmlerin yüzey morfolojileri farklılıklar göstermiş olup küresel, kümelenmiş ve tabaka şeklinde yapıların oluştuğu tespit edilmiştir. Agar difüzyon testi antibakteriyel aktiviteleri incelenmiş olup üretilen numunelere antibakteriyel etkinlik göstermediği görülmüştür. Bakteriyel yapışma ve hayatta kalma organizma sayımıda en yüksek yapışma oranının ise Ni katkısında olduğu görülmüştür.

2023, 49 sayfa

Anahtar Kelimeler: SILAR metot, Çinko oksit, Antibakteriyel aktivite

PREFACE AND ACKNOWLEDGEMENTS

I would like to thank my thesis advisor, Asst. Prof. Dr. İlker KARA, for his patience, guidance and understanding.

Mohamed Abdulhusein Mohsin AL-SUDANI
Çankırı-2023

CONTENTS

LIST OF SYMBOLS

A	Absorbance
Å	Angstrom
°C	Centigrade degree
Cs	Crystal size
d_{hkl}	Interplaner distance
d_{XRD}	Experimental distance
d_{CARD}	Standard distance
E_g	Energy band gap
E_{ph}	Phonon energy
eV	Electron volt
h	Planck's constant
I	Transmittance intensity
I_A	Absorbed intensity
I_R	Reflected intensity
I_o	Standard (Incidence) intensity
K	Kelvin
k_o	Extinction coefficient
k_B	Boltzman constant
M	Molar
$M_{(hkl)}$	Miller indices
nm	Nanometer
n_o	Refractive index
N	Complex refractive index
R	Reflectance
ν	Frequency
T	Transmittance
TCO	Transparent conductive oxides

LIST OF ABBREVIATIONS

EDS	Energy dispersive X-ray spectroscopy
FESEM	Field emission scanning electron microscope
UV-VIS	Ultraviolet-visible
XRD	X-ray diffraction

LIST OF FIGURES

LIST OF TABLES

1. INTRODUCTION

Biosensors are an essential part of the medical field, as well as the fields of environmental protection, energy conservation, food safety, chemistry, and agriculture. Because of the need to use continuous onsite monitoring that has both flexible and dependable qualities, biosensors have been proposed as an effective instrument for performing quick measurement and analysis (Elmer and White 2018).

However, during the course of the previous decade, a great number of articles were published that presented materials such as photonic crystals and metal organic frameworks that are being appropriate for use in biosensor applications (Nasrollahzadeh *et al.* 2019).

In comparison to bulk ZnO films, the use of nanostructured ZnO for biosensing applications has generated a significant amount of attention during the last several years. When compared to planar sensor designs, nanostructures have a number of advantages that are unique to them and show tremendous potential for quicker responses and better sensitivities (Hulla *et al.* 2015).

Nanostructures can have a variety of morphologies. ZnO nanoparticles have the potential to serve as superior fluorescence enhancing substrates, which makes them well suited for the detection of biomolecules (Duhan *et al.* 2017).

On the other hand, researchers have investigated a wide variety of ZnO nanostructures for use in biosensor applications. These nanostructures may be manufactured in a variety of different ways, including physical and chemical. İn which, ZnO nanostructures have a great potential for such studies. Thus, ZnO based matrices are an attractive candidate for use as the basis of low cost biosensors due to the simplicity with which they can be fabricated utilizing low cost techniques that can generate a broad variety of nanostructures. It is vital to further characterize these nanostructured materials in order to progress the field of electrochemical biosensors and get closer to the aim of developing a point of care diagnostic device that is sensitive, quick, and affordable (Silvestre *et al.* 2016).

1.1 Aim of Study

The study is focused on different techniques of strengthening the sensing properties of metal oxides by optimizing factors such as synthesis processes, morphology, composition, and structure. Specifically, the work is aimed at improving the sensitivity of the metal oxides.

2. LITERATURE REVIEW

2.1 Nanotechnology

To start, there is not yet a universally accepted meaning of the term "nanotechnology," despite the fact that it is gaining more attention in the scientific, regulatory, and public spheres. In general, nanotechnology in its most basic form, relates to the manufacturing, manipulation, and use of materials on a scale of one hundred nanometers or less. At this size, materials react surprisingly, displaying features that vary physically, chemically, and physiologically from their bigger counterparts. Besides, investing in nanotechnology has continued to rise as a direct consequence of the widespread consensus among academics and those in positions of power that this field represents the most promising direction for the future (Gehrke *et al.* 2015).

Although the field of nanotechnology research moves ahead at a rapid pace, there is little question that occupational and public exposure to nanoparticles that might be dangerous will rise. In which, innovation in nanotechnology applications is moving ahead of associated policy and legislation, which raises worries that research in areas such as ethics, the environment, the economy, the legal system, social issues, and toxicology is falling behind. The potential problems that might arise from the use of nanotechnology are almost as many and diverse as the advantages that it offers (Bhushan 2017).

In addition to the more usual concerns about health and safety, they include problems addressing conflicts between international, federal, state, and agency rules; concerns pertaining to intellectual property; and challenges relating to privacy. In the meantime, the Environmental Protection Agency (EPA) is taking a holistic approach to the issue of nanotechnology by researching potentially beneficial applications and developing risk assessment and management strategies (Alvarez *et al.* 2018).

On the other hand, researchers believe that engineered nanomaterials should be evaluated for their effects on human and environmental health in a manner distinct from that of their larger counterparts. This is due to the fact that engineered nanomaterials differ from their larger counterparts in terms of size, shape, surface area, chemical composition, and biopersistence (Prasad *et al.* 2017).

Cunsequently, the uncertainty that surrounds nanotechnology has left scientists, regulators, and the general public without clear guidance regarding the safety of these materials as their use becomes more widespread (Figure 2.1). Of course, there is a wide range of opinions that fall somewhere in the middle of these two positions, but the fact remains that this is the case such as using Carbon Nanotubes (CNT) (Nikalje 2015).

On the other hand, CNTs are a particular reason for worry due to the fact that they are already present in the environment in the form of soot, air pollution, and the consequences of combustion (Sanzari *et al.* 2019).

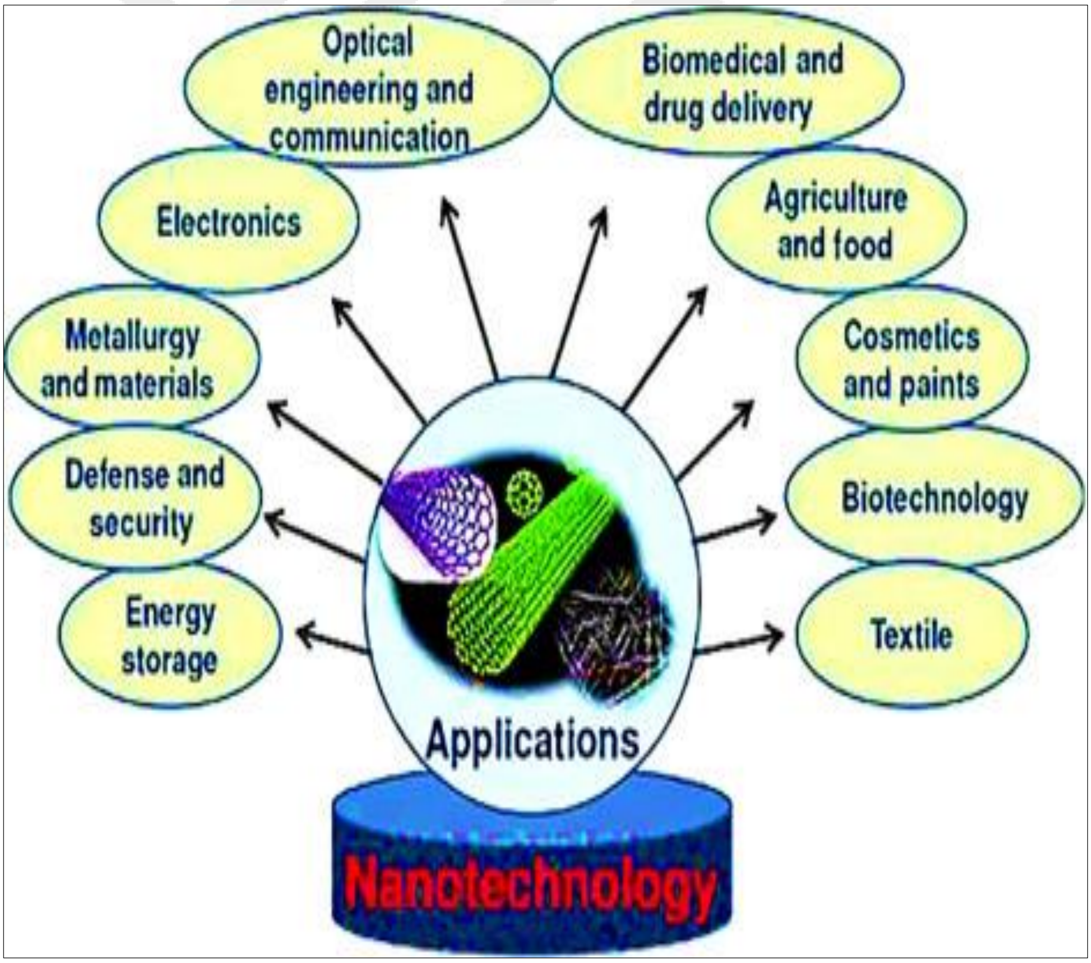

Figure 2.1 Application of nanotechnology (Zhang *et al.* 2019)

Moreover, because to their prevalence and the fact that they have been the subject of more risk assessment studies than other nanoparticles. This is because CNTs are more common than other nanoparticles. The risk of exposure by inhalation is of particular concern due to the ease with which nanoparticles may be released into the air and suspended from combustion sources, which can be either stationary or mobile. Also, larger particles have a greater propensity to linger in the upper respiratory airways after being inspired (de Francisco *et al.* 2018).

There have previously been a number of research on the respiratory toxicity of CNTs. On the other hand, all camps are in agreement that a deeper comprehension of the dangers posed by nanomaterials must first be attained before the numerous benefits promised by nanotechnology can be fully realized. Despite the fact that this might cause damage, ultrafine particles provide an even greater risk because of their capacity to penetrate deeper into the alveolar areas of the lungs, which are the regions in which gas exchange takes place. Because of this, determining the long-term effects of nanomaterials on human health has placed a priority on doing research on the toxicity of nanoparticles on the respiratory system (Pramanik *et al.* 2020).

In general, the methods for the synthesis of ZnO nanostructures may be broken down into two categories: those that are wet-chemical or solution-based, and those that are physical technique-based. Physical approaches, such as vapor liquid solid (VLS), vapor solid and chemical vapor deposition (CVD), in addition to thermal evaporation, often need high temperatures and pressures in addition to specialized substrates, and they typically result in a poor product yield. These procedures result in ZnO nanostructures of a high quality; nevertheless, the processes themselves are expensive and use a lot of energy. Processes that are hydrothermal or solvothermal, solution liquid solid (SLS) synthesis, capping agents, and surfactant-assisted synthesis are examples of wet-chemical or solution-based approaches (Grzybowski and Huck 2016).

The production of ZnO thin films has been accomplished by the use of a wide variety of techniques, including sputtering, thermal evaporation and condensation, solid state reaction, pulsed laser deposition (PLD), and chemical approach, amongst others. It is possible to fabricate ZnO thin films using a variety of chemical deposition methods, including CVD, electrodeposition, spray pyrolysis, and sol-gel deposition methods. These chemical deposition methods are accessible (Wang *et al.* 2016).

Herein, spray pyrolysis is the method of choice for the deposition of metal oxide films since it is straightforward, does not incur significant costs, and the manufacturing process can be quickly scaled up. Spraying the solution onto the substrate while it is being heated to a very high temperature is how this method is carried out. In the pyrolytic process, the temperature of the substrate is the parameter that acts as a controller for the grain size. This is because it is preferable to have a smaller grain size in order to increase sensor performance. Both the thermal evaporation technique and the Rf (Radio frequency) magnetron sputtering method are included in the physical pathway for the creation of a ZnO thin film. High purity, excellent repeatability, and precisely controlled thickness are all characteristics of the thin layer that may be created using the RF magnetron sputtering technology (Lowry *et al.* 2019).

On the other hand, nanomaterials may have very different physical and chemical characteristics depending on their size, shape, and the chemistry of their surfaces. Therefore, the development of new synthetic methodologies is very necessary for the production of innovative nanomaterials. For example, Zinc easily forms hydroxy and ammonia complexes, and the hydrolysis of such complexes is the basis for these procedures. In addition, the direction in which the development will occur may be adjusted using a variety of chemicals in these approaches. Citrate inhibits development in the c-direction and guides the crystal structure into thicker rods or even plates, while amine chemicals are often employed to drive growth in the c-direction (Hornyak *et al.* 2018).

Therefore, wet-chemical or solution-based approaches provide a route for the manufacture of the required ZnO nanostructures that is both convenient and easy to manipulate, has the ability to be scaled up, and can be accomplished at a lower temperature. The solution-based process that involves seed layer deposition and is then followed by ZnO growth is the technique that is used the most often when it comes to developing nanostructures. Electrochemical approaches have just recently emerged as a novel method for the fabrication of ZnO nanostructures (Manjunatha *et al.* 2016).

Quartz crystal thickness monitoring is a method that may be used to measure the thickness of the thin film. Because of the vibrations caused by the Zn-O bonding, the FTIR analysis used to characterize the ZnO layer on the SPR sensor produced a peak at a wavelength of about 418 and 550 cm. ZnO has a hexagonal wurtzite crystal structure, and an XRD pattern of ZnO thin film over an Au SPR sensor generates a peak at 2 = 34.1°. This peak is in accordance with the 002 plane of the structure. Based on this number, it can be deduced that the ZnO thin film that was produced is oriented along the c-axis. ZnO for the purpose of improving sensitivity Several methods for increasing sensitivity have been investigated as a result of the need for ultra-high sensitivity sensors for the detection of biological and chemical substances at low concentrations and tiny molecular weights. These sensors are required for the identification of the chemicals (Yetisen *et al.* 2016).

In the field of adhesion materials, furthermore, Chromium (Cr) and Titanium (Ti) are very popular choices. In spite of this, there are a few downsides, the most notable of which are metal interdiffusion and the minimal amount of light that is transferred to the surface of the gold layer. In addition, the FWHM value produced by these materials is rather huge, and they have a poor sensitivity. Titanium dioxide (TiO_2) and silicon dioxide are two examples of the metal oxides that are employed in the adhesive layer that is located between the substrate and the metallic layer (SiO_2) (Singh *et al.* 2017).

Plasmonic effects generated a light-trapping effect near the TiO_2/SiO_2 contact, which enabled the creation of additional surface plasmons. As a direct result of this, the resonance angle shift and therefore the SPR sensing were both improved. In addition, zinc oxide, which is a semiconducting metal oxide, has been employed as an adhesive material. This is due to the fact that zinc oxide has a non-centrosymmetric feature, which improves the sensor’s overall performance. The contact between ZnO and metal contributes to the promotion of phonon interaction (Usman *et al.* 2020).

2.2 ZnO:Usage and Its Properties

Zinc is a trace element that is absolutely necessary for the human body; without it, many enzymes, including carbonic anhydrase, carboxypeptidase, and alcohol dehydrogenase, become inactive. Because it can control a wide variety of physiological processes, it is essential to eukaryotic organisms. Bamboo salt, which contains zinc, is used as a herbal remedy for the treatment of inflammation (Weldegebrieal 2020).

Since the beginning of the 1900s, researchers have been doing research on ZnO, which is one of the semiconductors derived from II-VI compounds. Over the last few years, there has been a rise in interest in ZnO due to the fact that it may be used in a variety of applications. The direct and broad energy band gap of ZnO is 3.3 eV at 300 K, which contributes to its widespread usage in optoelectronic applications. These applications are the source of the current interest in ZnO. It is also highly beneficial since the method involved is straightforward and doesn't need a lot of money, and it can function well even under challenging working conditions. It is among the best materials for solar cells and flat instrument panels in terms of being a conductive metal oxide that is also permeable (Sinha *et al.* 2016).

ZnO thin films, both doped and undoped, find use in a variety of domains, including gas sensors, surface acoustic wave devices, and parts of optoelectronic circuitry. ZnO, which is transparent in the visible area, may be used in the production of green, blue-ultraviolet, and white light-emitting devices. This is one of the optoelectronic uses of the material. In addition, compared to other semiconductors (GaN with 25 meV and GaAs with 4 meV), the exciton binding energy of ZnO, which is 60 meV, is much higher. Because of this, it has a high binding energy at ambient temperature as well as higher temperatures, and it is dense towards the band edge (Karthik *et al.* 2022).

It is more resistant to radiation than GaN, and it exhibits piezoelectric, ferroelectric, and ferromagnetic characteristics, making it a multifunctional material. Today, zinc oxide may be manufactured by a variety of storage processes. Some of these processes are vacuum evaporation, reactive evaporation, sputtering, metal organic chemical vapor storage, and metal organic chemical vapor deposition. Sputtering is the most effective method for producing ZnO. Because single and well-oriented surfaces may be formed even when the temperature is low and the substrate is amorphous, which is very similar to the morphology of single crystals (Uikey *et al.* 2016).

Generally, the creation and use of such materials with dimensions of up to one hundred nanometers are the focus of the field of nanotechnology. They find widespread use in a variety of processes, including those pertaining to the fields of material science, agriculture, the food industry, cosmetics, medicine, and diagnostics. Because of their high surface area to volume ratio as well as their one of a kind chemical and physical properties, nanosize inorganic compounds have shown extraordinary antibacterial activity at extremely low concentrations. These particles are also less likely to be affected by changes in temperature and pressure when exposed to them. Some of them have been verified as being safe to consume, and some of them even include minerals that are required by the human body (Borah *et al.* 2019).

As a result of the proliferation of new bacterial mutations, antibiotic resistance, outbreaks of dangerous strains, and other related phenomena, the creation of antibacterial drugs that are more effective has become an urgent need. Bacterial infections are widely acknowledged to be a major public health concern across the world. Therefore, zinc oxide had antibacterial characteristics. Also, historical documents reveal that zinc oxide was used in a variety of ointments for the treatment of wounds and boils. This practice had been in use throughout the reign of the pharaohs (Suntako 2015).

When compared to other nanoparticles (NPs) of the same group of elements, zinc oxide nanoparticles have a higher level of activity against gram-positive bacteria (Aydin 2019). The relevance of semiconductor compounds belonging to the II-VI group is growing steadily due to the many benefits that these compounds provide to industry. In comparison to insulators and conductors, II-VI group semiconductor compounds exhibit distinct optical and electrical characteristics. In addition to existing as elements such as silicon and germanium, semiconductors can be produced in the form of binary, triple, or quaternary compounds due to the varied physical properties of these compounds and the ease with which they can be manufactured. Single and polycrystalline semiconductors are the most common types of semiconductors (Shohany *et al.* 2020).

However, the elements Si and Ge may be found in Group IV of the periodic chart. They are the semiconductor materials that make up the group and have been the subject of the greatest study; as a result, their characteristics are the most well-known. Compound semiconductors belonging to the II-VI group IV. They are considered to be more recent examples of the semiconductor material group elements. These materials may be created as multicrystalline layers of high quality using the necessary procedures, and they can be acquired in high purity owing to the low cost of the basic ingredients they are made from (Verma *et al.* 2017).

On the other hand, the energy gap in the band structure of II-VI compounds may range anywhere from 1.8 to 4 eV. It radiates in the visible range from the violet top all the way to the infrared spectrum, which demonstrates that it has an excellent luminescence quality. Because of their large band gap and direct-pass characteristics, they are used in the visible area of the electromagnetic spectrum in devices like as LEDs and photodetectors. In addition to this, the majority of these compounds have a very high level of carrier ion entrainment in the energy band gap and are very good at transmitting electrical energy. These compounds, particularly those consisting of zinc and cadmium, are the subject of a significant amount of study and inquiry. This is due to the fact that they are suitable for use in optoelectronic applications and that their manufacturing stages are quick and sophisticated. Compounds II-VI that can be made into semiconductors; It is possible to find hexagonal, cubic, and zinc sulfide crystal phases when it crystallizes (Figure 2.2) (Saranya *et al.* 2016).

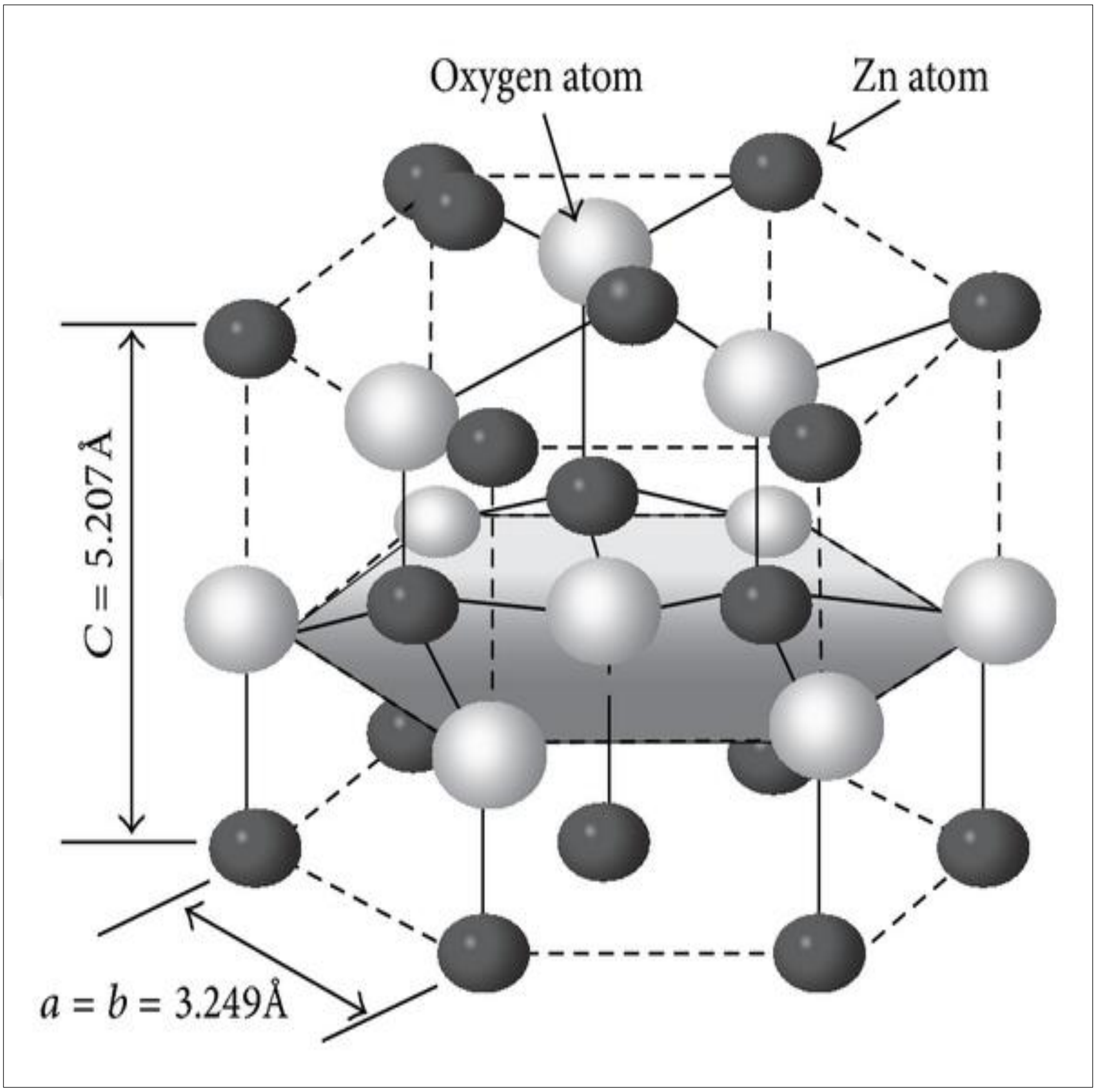

Figure 2.2 Structure of ZnO (Manoj *et al.* 2021)

2.3 Defects in ZnO

ZnO is susceptible to the same kinds of point flaws that impact the electrical and optical characteristics of other semiconductors. Calculations were made utilizing the plane wave pseudopotential technique in conjunction with the Kohen and Walve supercell methodology in order to determine the electronic structure of ZnO as well as the production energy of hydrogen and native point defects. generally, the concentration of the defect in the crystal is shown to be dependent on the energy of formation, denoted by Ef (Ranjith and Kumar 2017).

However, the results of the calculations for O and Zn vacancies, intermediate atoms, and misplaced atoms in ZnO are shown in Figure 2.3. The calculations were performed using two different limiting chemical potential values. There are two distinct outcomes that might occur in ZnO wrtzite. The tetrahedral order comes first, followed by the octahedral order. The last of these is the icosahedral order (Wang *et al.* 2021). O and Zn vacancies are the two types of ZnO defects that are seen most often.

For instance, the amount of energy required to produce oxygen vacancies (VO) (Zni) is much less than the amount of energy required to form intermediate atoms. As a result, there is a much higher concentration of zinc atoms. In an atmosphere with a high concentration of oxygen, zinc vacancies (V_{Zn}) may predominate. In terms of the electronic properties of ZnO's basic point defects, the oxygen vacancies are classified as a kind of defect known as a negative - U defect (Hasnidawani *et al.* 2016).

Because as the Fermi level rises, a shift from the +2 state to the neutral state takes place. In n-type zinc oxide, the zinc vacancy is predicted to have a charge of minus two. At a potential difference of about 0.8 eV above the valence band, V_{Zn} makes the transition between its -1 and -2 charge levels. Because of this, n-type ZnO emits a wide green luminescence, which is one of the factors that leads to V_{Zn}. This is comparable to the theory that the yellow luminescence in GaN results from negatively charged Ga vacancies being present in the material. It is believed that the +2 level of oxygen vacancies occurs about 2.7 eV higher than the valence band. This is due to the fact that the positive charge state of VO is an unstable condition (Nayak *et al.* 2022).

In prior investigations, hydrogen in ZnO has also been examined. When compared to the hydrogen in other semiconductors, the hydrogen in ZnO always acts as a donor and has a positive charge. ZnO has a 1 Å long OH bond, which holds hydrogen in very close proximity to oxygen. 1.56 eV is the amount of energy required for the production of hydrogen in n-type ZnO. The combination of hydrogen is seen as having a greater potential for success in p-type ZnO. In point of fact, this may be useful in order to produce p-type zinc oxide. The composition of hydrogen during development raises the acceptor solubility, and the method of doping GaN with Mg acceptor is analogous to the behavior of hydrogen (Figure 2.3). After that, the annealing process, which involves the elimination of hydrogen, may help to alleviate the issue (Sadhukhan *et al.* 2019).

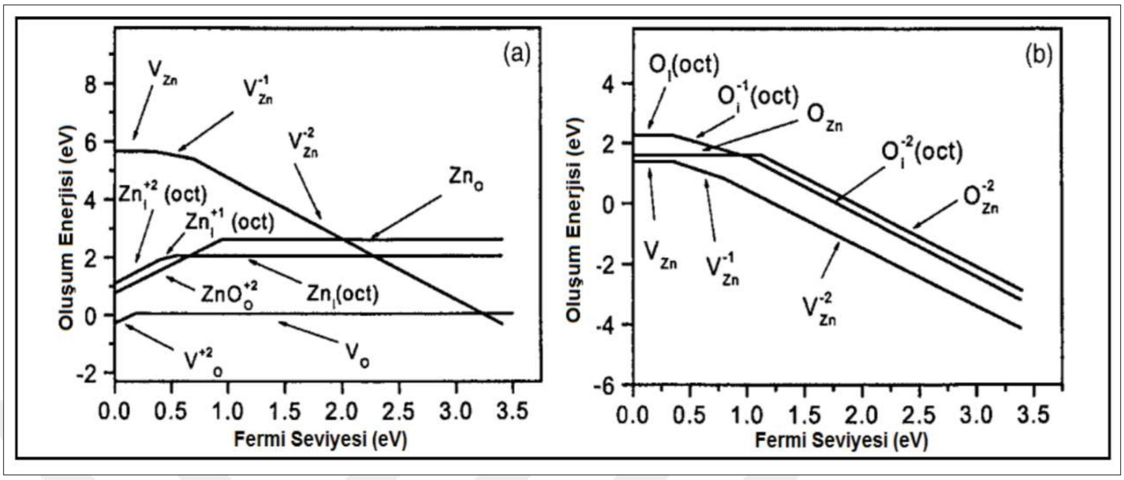

Figure 2.3 Defect formation energy for fundamental natural defects, a) zinc rich conditions, b) oxygen rich conditions (Raizada *et al.* 2019)

2.4 Crystal Structure

The mineral zinc was discovered by Bruce In Franklin in 1810. It is mostly red or orange with manganese impurities present in zinc. The photograph of zinc is shown in Figure 2.1. Zinc oxide crystals exhibit many types of surface orientation. The most important surface orientations are (0001) and (000-1) fundamental plane, (10-10) and (11-20) prism planes, (11-21) pyramid planes crystal surfaces (Zagorac *et al.* 2019).

The tetrahedral coordination is typically sp^3 covalently bonded, but these materials also have an important ionic character. ZnO is an II-VI group compound semiconductor whose ionic character is between covalent and ionic semiconductors. The thermodynamic phase at ambient conditions is wurtzite. Zinc sulfide ZnO structure is only achieved by growing on cubic subbases. At high pressure, it shows the properties of rock salt (Figure 2.4) (Sheldrick 2015).

Figure 2.4 (a) Orange zinc crystal from the Sterling (Ogdensburg, USA) mine, (b) synthetic zinc oxide crystal (Gushurst *et al.* 2019).

In addition to the hexagonal wurtzite phase, the rock salt structure and the unstable cubic phase are also known. The cubic phase transition of ZnO at 300 K and 9.8 GPA pressure exhibits rock salt (NaCl) structure formation. This means that the high pressure phase is not stable at normal pressure (Burla *et al.* 2015).

2.5 Knitting Parameters

In general, high-resolution X-Ray diffraction with symmetrical and asymmetrical reflections using the Bond technique is the most popular and accurate way for measuring the lattice parameters of any crystal metal. This approach is also considered to be the most exact. In general, the following factors list the importance to determine how the lattice parameters of a semiconductor are determined (Senthil *et al.* 2018):

1. The concentration of free electrons that emerge via the deformation potential of a minimum conduction band that is surrounded by free electrons. The concentration of foreign atoms and defects (Rotzler *et al.* 2022).
2. External stresses. The concentration of free electrons that emerge via the deformation potential of a minimum conduction band that is surrounded by free electrons (eg, induction by the subbase).
3. Temperature Several alternative approaches may be used in order to ascertain the hexagonal unit cell's lattice characteristics. The range of values for the a parameter at room temperature is between 0.32501 and 3.32475 nm, while the range of values for the c parameter is between 0.52042 and 0.52075 nm (Yibar *et al.* 2022).

Herein, the values a = 0.32495 nm and c = 0.52069 nm are those that are most often used for fixed parameters. The density comes in about 5,605 g/cm^3. The optimal structure for wurtzite is a hexagonal structure with two lattice parameters (a and c), and the ratio between these two parameters is 381.633. A actual ZnO crystal will have a wurtzite structure that deviates from the ideal order due to variations in the c/a ratio. The degree to which the actual wurtzite crystal structure deviates from the ideal one is determined by the lattice stability and ionicity of the material. The value of the lattice constant increases when there are point defects as well as growing flaws (Peiner *et al.* 2022).

2.6 Electronic Tape Structure

To begin, Wrtzite has ZnO in its crystal structure. The structure of a vurtzite mineral is characterized by a hexagonal unit cell that has two lattice parameters, denoted a and c. Within the hexagonal brillon zone, the band structure was shown along planes with a very high level of symmetry. The maximum of the conduction band and the lowest of the conduction band occur at the point Γ. ZnO is a direct bandgap semiconductor, as shown by the fact that it has a point at K = 0. It was discovered by analyzing in Figure 2.3 that wrtzite constitutes the electrical structure of ZnO. The results of the calculations show that the band structure value of ZnO (0.067 Ryd) is 0.91 eV [at 0 K], which is in accordance with the findings that have been published in the scientific literature. The numbers a = 0.3227 nm and c = 0.5189 nm have been determined to be those of the equilibrium lattice parameter 18 for ZnO. These values are congruent with the other values (Singh *et al.* 2016).

Furthermore, the majority of the electrons end up near the edge of the valence band. In most of the valence and conduction band, the findings are shown as sp^3 d^5 for Zn and p^3 for O. The top partitions of the surface state density originate from the s, p and d orbitals of zinc, whereas the bottom partitions come from the s and p orbitals of oxygen. Nevertheless, these states exhibit a considerable amount of mixing between the p and d states of zinc. The following is a list of some of the most prevalent kinds of electrical and electronic tape that are used in industrial applications (Tiwari *et al.* 2018, Laguna-Marco *et al.* 2015, Einollahzadeh *et al.* 2016, Römelt *et al.* 2017):

1. The ability of black vinyl tape to resist a broad variety of elements has established it as the industry norm for insulation system and isolation. Despite its tremendous strength and longevity, it may be quickly removed and leaves behind very little or none of a residue when it does so. It also demonstrates good UV resistance.
2. Thermal Insulating Tape: This type of electrical isolation tape is employed to maintain high away the heat from hardware, such as wires, cables, and hoses, and on or near equipment that poses a fire hazard, such as engines and furnaces. Other uses for this tape include keeping high heat away from equipment that could cause an explosion, such as equipment that could start a fire. It becomes sticky when heated, which enables the tape to have increased adhesive flexibility. When the tape is cooled, it becomes much simpler to adjust or remove sections while it is being assembled.
3. Tape for Heat Sealing: This kind of tape is used on equipment that are capable of reaching very high temperatures, such as vacuum sealers. It creates a barrier between the source of heat and other items, so preventing those other objects from melting.

4. Acetate Cloth Tape: Acetate cloth tape has good adhesion and insulating qualities, is visually pleasant, and has outstanding conformability in coil-wrapping applications. Additionally, it has the capacity to absorb varnishes and varnishes.
5. Electrically Conductive Adhesive Tape: Electrically conductive adhesive tape offers dependable electronic isolation by assuring that there is no direct connection between two or more circuits or nearby components. This kind of tape may be used in a variety of applications. This tape is put to use in a wide number of applications across many different sectors, including the electrical, medical, and pharmaceutical ones.
6. Insulation Tape for Electrical Circuits Insulation tape for electrical circuits offers the adaptability and dependability necessary for important applications by reducing overvoltage and isolating any circuits that, if linked, may be harmful.
7. Paper Electronic Tape Manufacturers of "through-hole" electronic components have a variety of in-processing and packaging requirements that may be met using paper electronic tape. It is used in a variety of applications including end-turn taping, banding coils, and covers for bobbin-wound coils.
8. Paper Masking Tape: This kind of tape was developed to provide temporary bindings during the installation of electrical components in various building projects. Die-cutting is another application that makes use of it.
9. Silicone Solid Rubber Tape Silicone solid rubber tape is created in a variety of formulations, each of which provides a unique set of features. These properties include resilience to severe temperatures, good tensile strength, and superior tear resistance, amongst others.
10. Composite Bonding Tape: Depending on the kind that is used, composite bonding tape exhibits a number of features. Some of these properties include resistance to heat, chemicals, and electricity; a low coefficient of friction; abrasion resistance; and conformable release surfaces.

2.7 Mechanical Properties

The mechanical properties refer to the material's resistance to the effects of these forces. For the purpose of determining how a metal reacts when subjected to a load, mechanical qualities such as strength, hardness, elasticity, brittleness, and softness, as well as twenty piezoelectric constants, are utilized as measures. Therefore, the changes that occur in the form of the material as a result of the impact of external forces are referred to as the material's mechanical properties (Akinwande *et al.* 2017).

These characteristics are characterized by the manner in which the metal is able to withstand forces and stresses (Hanzl *et al.* 2015). There are four distinct elastic constants that may be found in hexagonal crystal formations, wich will be discused below (Ma *et al.* 2015).

2.8 The Structre of Enzyme-Based Biosensors

Figure 2.5 illustrates the breakdown of a biosensor structure into a biotransducer and its supporting signal processing components (Yin *et al.* 2018). These substances cause the target analyte and the transducer to interact physicochemically, resulting in signal impulses being sent to the signal processor. The compatibility of metal oxide inorganic materials with organic materials is a significant challenge (Wang *et al.* 2019, Yilmaz *et al.* 2020).

ZnO-based Biosensors are direct wide band gap semiconductors that display n-type conductivity when exposed to UV radiation. During crystallization, wurtzite takes on a hexagonal configuration (see Figure 2.5), which is based on noncentrosymmetric crystal formations and possesses unique piezoelectric capabilities. Wet approaches make up the majority of the ZnO production processes (Yuea *et al.* 2020). Future medical uses of biosensors will require better biological entity binding than tin oxide, which ZnO possesses (Lei *et al.* 2011). ZnO can be used as a permanent human sensor in chronic conditions like diabetes because it is harmless and compatible with human skin. ZnO nanostars were produced using Chemical Bath Deposition (CBD) and utilized to detect micro RNA-21 in cancer cells. When creating Electro Chemi Luminescence (ECL) biosensors, the surface was previously functionalized via thiolmodified hairpin and hybridization chain processes (Faria and Mazon 2019).

Additionally, MOS biosensors can be employed for early viral detection. The hydrothermal process is another method that has been widely employed for ZnO production with applications in biosensing. Hydrothermally produced ZnO nanoparticles and nanorods were both utilized in biosensors for the detection of glucose (Zong and Zhu 2018). When compared to ZnO nanopowder functionalized with GOx, where LOD was 50 M, these results are noticeably superior. ZnO nanorods were produced hydrothermally and employed as G-Immunoglobuline and phosphate sensors. (Dong *et al.* 2017).

This is why functionalizing MOS (i.e., TiO_2, WO_3, SnO_2, and ZnO) to boost its compatibility with organic materials has garnered a lot of attention. The advantages of the metal oxide semiconductors for immobilizing biomolecules (Ramon-Marquez *et al.* 2018, Zhao *et al.* 2019) include: (a) their high isoelectric point (IEP), which induces electrostatic attraction forces with many biomolecules with lower electrostatic points; and (b) their morphological versatility, demonstrated by a high surface area to volume ratio typical of nanomaterials and helpful for immobilizing enzymes (Fiorani *et al.* 2019).

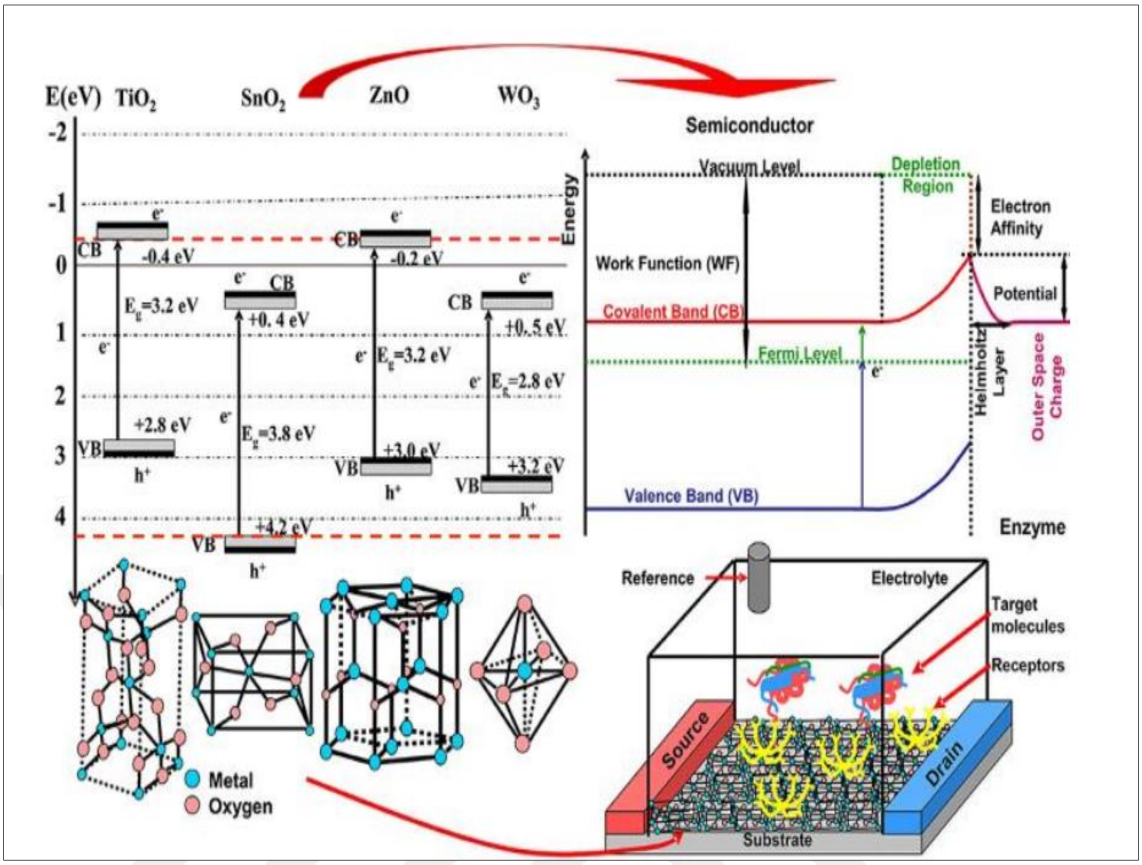

Figure 2.5 Band energies, crystalline structure, and biosensor configuration of MOS utilized in biosensors

Acetylcholinesterase was used as a functionalizing agent in the pesticide detection process using the SnO_2 nanoparticles produced by sonication procedures. (Wang *et al.* 2018). For methyl parathion and carbofuran, the LOD determined by cyclic voltametry (CV) was 5×10^{-14} and 5×10^{-13}, respectively (Zhou *et al.* 2013).

To create SnO_2 nanoparticles for the purpose of detecting H_2O_2, the microwave irradiation approach was used (Dong and Zheng 2014). SnO_2 surface was functionalized with HPOx and, based on differential pulse voltammetry (DPV), a LOD of 43 nM was obtained (Lavanya *et al.* 2012). SnO_2 nanowires made through thermal evaporation were used to create an H_2O_2 sensor. (Li *et al.* 2010).

The LOD determined by CV was 0.8 μM using the same functionalizing molecule as SnO_2 nanoparticles. The electrospinning technique was also used to produce SnO_2

nanowires for glucose amperometric detection (Alim *et al.* 2019). The troponin I detector, a protein marker for myocardial infarction, was successfully employed with the nanobelts functionalized with Dbiotin molecules (100 pM LOD). The amyloid-protein (A) was detected using the nanosheets following a previous functionalizing step involving an anti-A antibody(Cheng *et al.* 2011). The LOD value was 0.17 pg/mL based on photocurrent measurements, which is regarded as promising for use in applications for the detection of disease-related biomarkers. (Zhang *et al.* 2019).

However, the LOD was shown to be 18.6 aM, which qualifies this substance as a promising candidate for a clinical bioassay. ZnO nanoparticles were created using the same method to detect the Zika virus in undiluted urine. The Zika virus causes symptoms including headaches, arthralgia, myalgia, or conjunctivitis and is spread by mosquito bites. The ZnO nanoparticles, the ZIKV-NS1 antibody was immobilized using glutaraldehyde and cystamine. When the LOD was assessed using CV, the outcome was 1,00 pg/mL (Faria and Mazon 2019).

The final step was functionalizing phosphate detection of ZnO using pyruvate oxidase via immersion, and the LOD was 0.5 μM. By immersion and cold drying, the ZnO surface was functionalized with myoglobin to create a G Immunoglobuline Sensor with 0.03 ng/mL LOD. The hydrothermal method was used to create ZnO nanocone arrays for dopamine detection (Ahmad *et al.* 2017).

2.9 Scanning Electron Microscope (SEM)

Electrons interact with the atoms in the sample to produce a variety of signals that reveal details about the sample's surface topography and composition. An image is created by combining the position of the electron beam with the strength of the signal being detected while it is being scanned in a raster scan pattern. Any sample's elemental composition can be determined using energy-diffusing X-ray analysis (EDS). EDS is a technique generally used in SEM device.

In this thesis study, SEM and EDS measurements of thin films produced by using the Hitachi SU 5000 Field Emission device, the photo of which is given in Figure 4.1, were made at room temperature in the Central Laboratory of Yıldırım Beyazıt University, as it does not require surface coating (Figure 2.6).

Figure 2.6 Hitachi SU 5000 field emission Scanning Electron Microscope (SEM)

3. MATERIALS AND METHODS

3.1. Materials

3.1.1 Samples used in the study

In this study, metal samples, which were integrated into the ITO surface ((a) undoped ZnO, (b) Ni-doped ZnO, (c) Al-doped ZnO) were used. Thin films were produced using the SILAR method (Figure 3.1).

3.2 Methods

3.2.1 SILAR Method

SILAR is a method that does not require cheap, high-quality surfaces and can work at room temperature without requiring vacuum. SILAR can be used at room temperature or close to room temperature and in various base materials such as semiconductors, metals, insulators. The parameters required to obtain good quality thin films with SILAR are to regulate the preparation conditions such as the number of cycles, rinsing time, concentration and adsorption of solutions. In this thesis study, the samples were enlarged by SILAR thin film magnification method.

3.2.2 Growth of ZnO Thin Films

The zinc-ammonia ($[Zn(NH_3)_4]^{2+}$) complex is used for the growth of ZnO thin films. To prepare the zinc-ammonia complex, 0.1M $ZnCl_2$ (pH≈5.5) and 25 - 28 % NH_3 solutions are mixed in the molar ratio [Zn:NH_3 =1:10]. $ZnCl_2$, $NiCl_2$ $AlCl_2$ and NH_3 solutions were mixed and Ni-doped ZnO (1 %) and Al-doped ZnO (1 %) solutions were prepared. The mechanism of growth of ZnO thin films by the SILAR method is shown schematically in Figure 3.1. The chemical reactions that take place during the growth phase are given below Equation (3.1-3.4):

$$ZnCl_2 + 2NH_4OH \leftrightarrow Zn(OH)_2 + 2NH_4^+ + 2Cl^- \tag{3.1}$$

$$Zn(OH)_2 + 4NH_4^+ \leftrightarrow [Zn(NH_3)_4]^{2+} + 2H_2O + 2H^+ \tag{3.2}$$

$$[Zn(NH_3)_4]^{2+} + 4H_2O \rightarrow Zn(OH)_2\,(s) + 4NH_4^+ + 2OH^- \tag{3.3}$$

$$Zn(OH)_2\,(s) \rightarrow ZnO(s) + H_2O \tag{3.4}$$

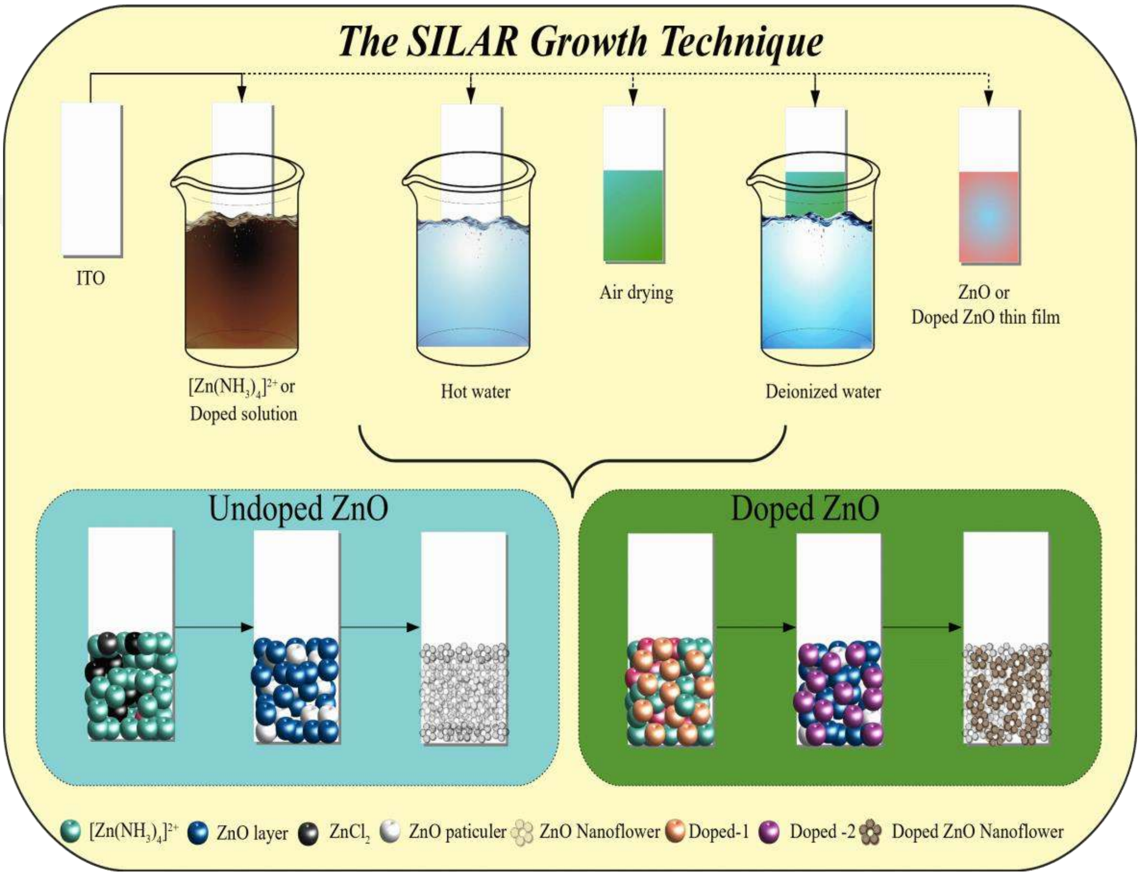

Figure 3.1 SILAR method techniqe

3.2.3 Annealing process

It was annealed in a nitrogen gas environment for 13 minutes at temperatures of 300 °C in an annealing furnace (Figure 3.2).

Figure 3.2 Annealing furnace

3.2.4 Determination of antimicrobial activity

Antimicrobial activities of the samples were determined by two different methods. Firstly, antimicrobial activities of the powder samples against Gram-negative (*Escherichia coli* ATCC 35218) and Gram-positive (*Staphylococcus aureus* ATCC 25923) pathogenic bacteria were determined by the agar well diffusion method (Reinheimer *et al.* 1990, Ibrahim Al Ahadeb 2022).

Test bacteria were grown in Nutrient broth (Merck) and their density was adjusted to McFarland 0.5. 100 µL of individual test bacteria were transferred onto the Nutrient solid medium and the bacteria inoculated on the medium were homogeneously dispersed. Then, wells with a diameter of 7 mm were opened on the solid medium with a sterile swab. 100 µL of samples at different concentrations (10, 25, 50, 100, 250, 500, 1000, 1500, 2000, 3000, 4000, and 5000 µg/mL) were added to the wells drilled in separate plates and incubated at 37 °C for 24 hours. At the end of the incubation, the diameter of the zones formed around the well was measured with a calliper and the results were given in millimetres. All studies were performed in 3 repetitions (Figure 3.3).

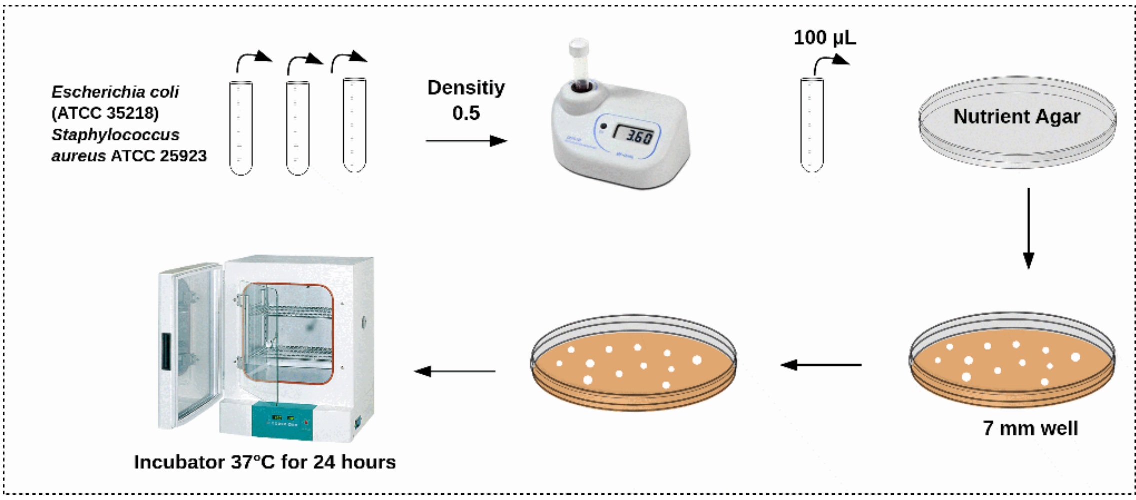

Figure 3.3 Agar well diffusion antimicrobial activity method steps

The second method is similar to the first method, the test bacteria (*E. coli* ATCC 35218, *S. aureus* ATCC 25923) density was adjusted to McFarland 0.5. Individual test bacteria were transferred (100 µL) onto the Nutrient solid medium and dispersed homogeneously. Then, different metals ((a) undoped ZnO, (b) Ni-doped ZnO, (c) Al-doped ZnO) were integrated into the glass surface, which was cut into small pieces, and placed on the test bacteria. Incubated at 37 °C for 24 hours. It was determined if there was any zone created at the end of the incubation period.

3.2.5 MIC and MLC/MBC analysis

The smallest concentration required to stop bacterial growth is known as the Minimum Inhibitory Concentration (MIC). The Minimum Lethal/Bactericidal Concentration (MLC/MBC) is defined as the minimum concentration at which no growth occurred in the medium (Al-Mijalli *et al.* 2021).

Bacteria samples were grown in Nutrient broth and their density was adjusted to McFarland 0.5 (~1.5×10^8 CFU/mL). Solutions containing powder metals at different concentrations (10 - 5000 µg/mL) were prepared. 50 µL of bacteria, 50 µL of metal and 100 µL of Nutrient medium were inoculated in 96 well plate wells and incubated at 37 °C for 24 hours. At the end of the incubation period, 10 µL was taken from the wells and dropped onto Nutrient agar. It was re-incubated at 37 °C for 24 hours. All studies were performed in 3 repetitions. In the study, the bacteria were used as the positive control while the metal was used as the negative control.

3.2.6 Survival organism counting method

The lid of the Petri dish was covered with coarse blotting paper and moistened with water. The metal samples integrated into the glass surface were placed in a standard petri dish with damp filter paper on the lid. 100 µL of the bacterial solution was placed on the glass samples cut into small pieces and incubated at 37 °C for 24 hours (Vartiainen *et al.* 2005).

After the incubation, the samples were taken into the tube containing phosphate-buffered saline (PBS) (0.02 % KCl, 0.144 % Na_2HPO_4, 0.8 % NaCl, 0.024 % KH_2PO_4, pH 7.0) solution to determine the number of viable bacteria on the surfaces. Vortexing was applied for 5 minutes to transfer the bacteria on the surface to the solution. After serial dilution using 0.875 % NaCl, 100 µL of bacteria was added to the Nutrient solid medium, the spreading plate method was applied and left in an oven at 37 °C for 24 hours. At the end of the waiting period, the colonies that grew in the petri dishes were counted and the number of viable bacteria was calculated according to the Equation (3.5-3.6) below.

$$\text{Number of Viable Bacteria } \left(\frac{\text{CFU}}{\text{mL}}\right) = \frac{(\text{Number of colonies x Dilution factor})}{(\text{Bacteria planted in petri dish (mL)})} \tag{3.5}$$

$$\text{Dilution factor } = \frac{1}{\text{Dilution ratio}} \tag{3.6}$$

3.2.7 Determination of bacterial adhesion

Cut into small pieces, the metal samples integrated into the glass surface were placed in a sterile petri dish. On each sample, 1 mL of bacteria from the bacterial culture whose density was adjusted to McFarland 0.5 was added and kept at 37 °C for 4 hours. At the end of the waiting period, a gentle wash with PBS was applied three times in order to completely remove the bacteria that did not adhere to the glass surface (Chua *et al.* 2008).

Then, the samples were taken into 1-2 mL of PBS and kept in an ultrasonic bath for 2 minutes to allow the bacteria on their surfaces to pass into the solution, and then vortexed for 1 minute. This process was tried in 3 different ways, by applying sonication (2 min) instead of an ultrasonic bath and without applying any physical processes. After serial dilution using 0.875 % NaCl, 100 µL of bacteria was added to the Nutrient solid medium, the spreading plate method was applied and left in an oven at 37 °C for 24 hours. At the end of the waiting period, the colonies that grew in the Petri dishes were counted and the number of viable bacteria was calculated.

4. RESULTS AND DISCUSSION

4.1 Morphological Properties of ZnO Thin Films

Undoped ZnO, Al-doped ZnO and Ni-doped ZnO samples produced in the SILAR method in 40 cycles were annealed at 300 °C. Morphological and elemental analyzes of thin films of produced undoped ZnO, Al-doped ZnO and Ni-doped ZnO samples were made.

SEM images of the produced undoped ZnO, Al-doped ZnO and Ni-doped ZnO thin films are given in Figure 4.1. Morphological analysis of undoped ZnO, Al-doped ZnO and Ni-doped ZnO thin films produced from SEM images can be performed. Morphological structures tend to be spherical in the undoped ZnO sample. However, the particles formed have an irregular structure. It has been observed that global structures tend to cluster together by forming larger structures.

When the surface morphology of the undoped ZnO sample is examined, the structures formed tend to be irregular and spherical The globular structures formed tend to cluster in some regions by forming larger structures. The surface morphology of the Al-doped ZnO sample shows an inhomogeneous structure as cavities, clusters on the surface. When the morphological structure of the Ni doped ZnO sample is examined, it is seen that it is homogeneously completely covered on the ITO surface. In addition, it is seen that there are some fractures on the surface, which is thought to be due to surface tension.

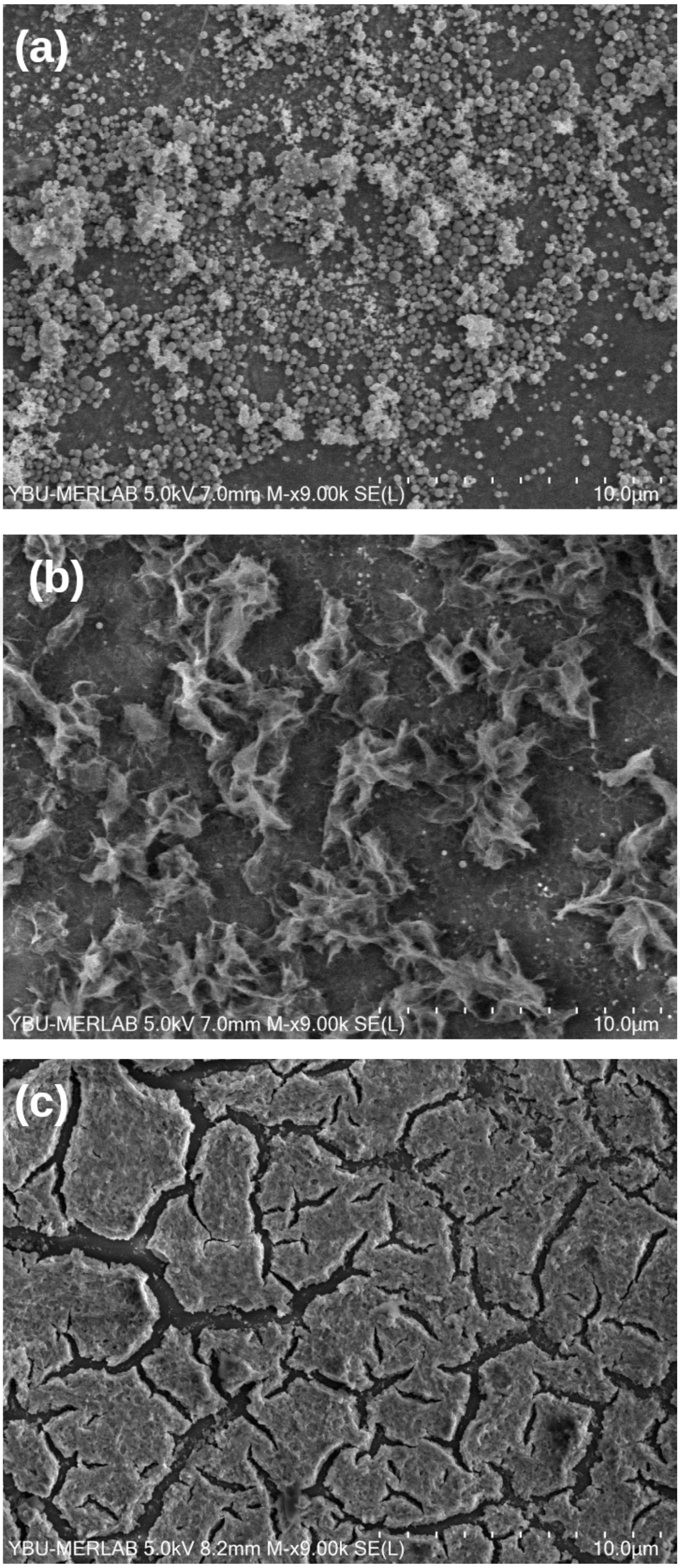

Figure 4.1 SEM analysis of (a), undoped ITO/ZnO (b) Al-doped ITO/ZnO, (c) Ni-doped ITO/ZnO thin films thin films

The EDS images of the produced undoped ZnO, Al-doped ZnO and Ni-doped ZnO thin films are given in Figure 4.2.

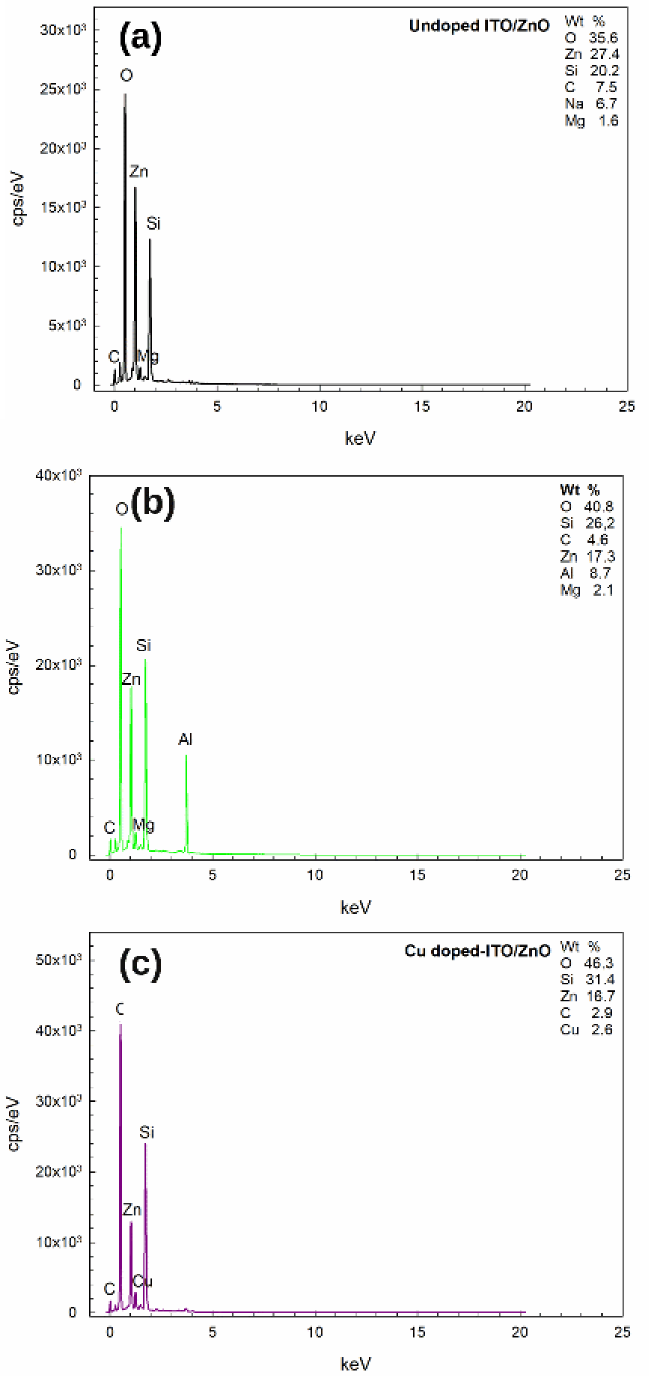

Figure 4.2 EDS analysis of of (a), undoped ITO/ZnO (b) Al-doped ITO/ZnO, (c) Ni-doped ITO/ZnO thin films

The ratios of Zn, O, C, Al, and Ni elements in the samples alter when the EDS analyses are reviewed, and these changes depend on the additive ratio. The substrate material is to blame for the occurrence of Si and C elements in EDS analyses. Na is a substance that exists because of an unwanted impurity.

4.2 Antimicrobial Activity

According to the results of the analysis, while no zone formation was observed at low metal concentrations, it was determined that both the zone formation and the size of the zone diameter generally increased depending on the increasing concentration. Zone diameters against *S. aureus* and *E. coli* bacteria were determined as 20.38 and 2.50 mm, respectively. Zone formation against pathogen bacteria was observed at 1000 µg/mL of Al, and Ni, metals, but it was not detected that they did not show any antibacterial effect at higher metal concentrations, see Table 4.1.

Table 4.1 The zone diameters (mm) of the bacteria

Metal	*E. coli* ATCC 35218											
	Concentration (µg/mL)											
	10	25	50	100	250	500	1000	1500	2000	3000	4000	5000
Al	-	-	-	-	2.92±0.01	4.04±0.03	4.37±0.01	-	-	-	-	-
Ni	-	-	-	-	-	-	4.00±0.01	-	-	-	-	-
Zn	-	-	-	-	3.47±0.00	4.80±0.02	7.46±0.05	9.42±0.01	12.10±0.01	13.16±0.06	13.73±0.03	17.52±0.01
***S. aureus* ATCC 25923**												
Al	-	-	-	-	-	-	-	-	-	-	-	-
Ni	-	-	-	-	-	-	4.00±0.01	-	-	-	-	-
Zn	-	-	-	-	-	-	10.34±0.01	10.40±0.04	14.79±0.03	15.74±0.03	16.48±0.06	20.38±0.01

* From the mean diameter ± SD, the mean surface area of the inhibitory zone was computed for each.

Exhibited zone formation of different concentrations of Ni and Al metal against *E. coli* and *S. aureus* were shown in Figure 4.3.

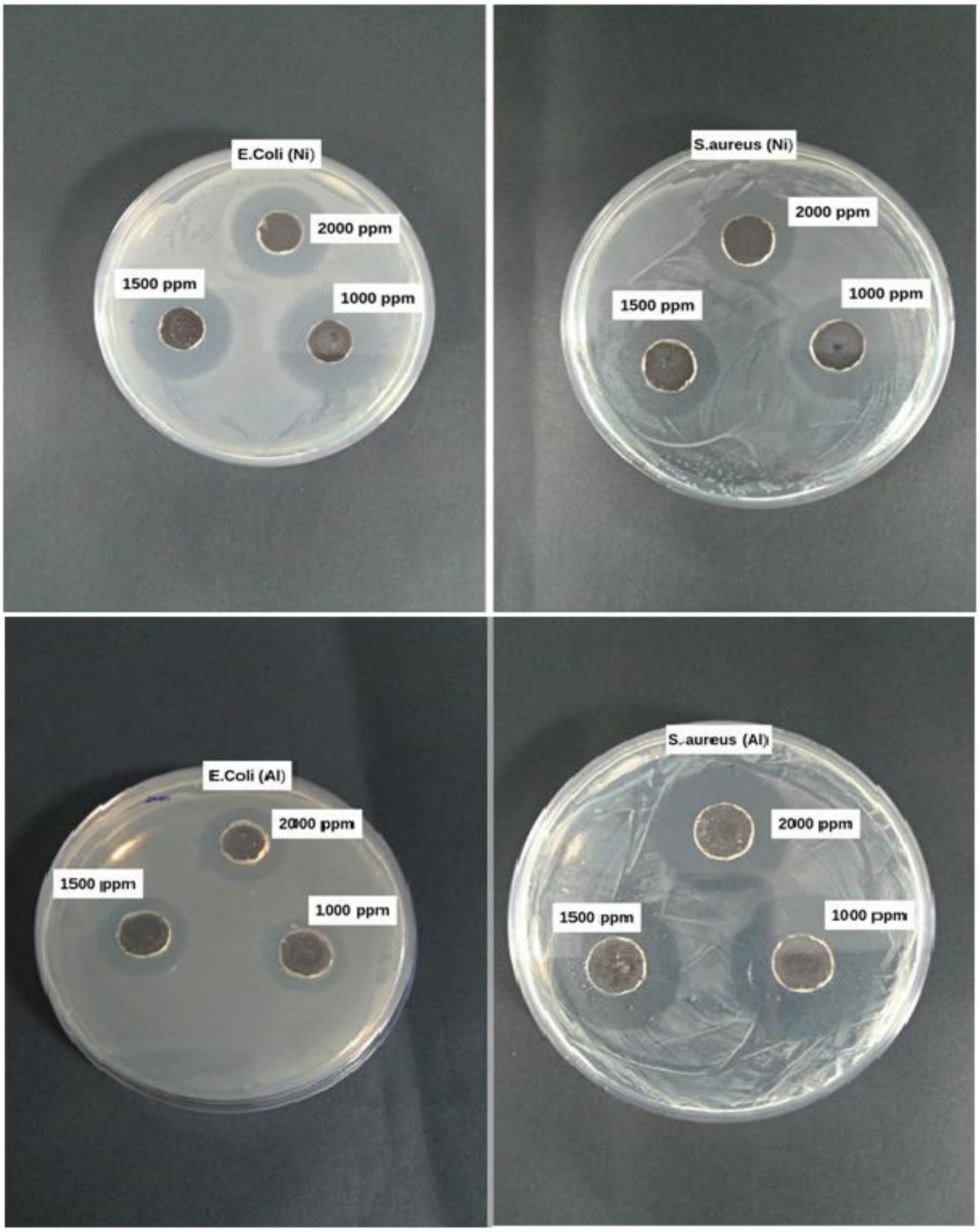

Figure 4.3 Zone formations of Ni and Al metal at different concentrations

Danial *et al.* (2020) synthesized undoped and in-doped (1, 3, 5 %) ZnO nanoparticles by sol-gel technique. Antibacterial activities of undoped and in-doped ZnO NPs were determined using the disk diffusion method. The human pathogenic bacteria, two Gram-positive bacteria (*Bacillus subtilis* NRRL-B-4219, and *Staphylococcus aureus* ATCC 25923) and two Gram-negative microorganisms (*Escherichia coli* ATCC 25922 and *Pseudomonas aeruginosa* NRRL B23 27853) were used for antibacterial activity.

The zone diameters of the bacteria used in un-doped ZnO and in-doped ZnO were determined as 12-15 mm and 12-18 mm, respectively. The highest zone diameter was obtained by *B. subtilis* NRRL-B-4219 in 5 % in-doped ZnO (18 mm) medium. In another study, the bulk SnO_2 nanoparticles and SnO_2 nanoparticles were tested for antimicrobial activity against to *E. coli* ATCC 25922 and *B. subtilis* UPMC 1175. Zone diameter against to *E. coli* ATCC 25922 was found 3 mm for bulk SnO_2 nanoparticles while 5-9 mm for SnO_2 nanoparticles.

Zone diameter against to *B. subtilis* UPMC 1175 was found 5 mm for bulk SnO_2 nanoparticles while 9-22 mm for SnO_2 nanoparticles. The highest antibacterial activity was observed against *B. subtilis* UPMC 1175 with the highest inhibition zone of 22 mm (Al-Hada *et al.* 2018).

In a second method, in which antimicrobial activities of different metals (undoped ZnO, (b) Ni-doped ZnO, (c) Al-doped ZnO) integrated into glass surfaces were determined against test bacteria, no zone formation was observed around the glass surface (Figure 4.4). This shows that the metals integrated into the glass surface do not have an antibacterial effect against the test bacteria, in other words, the pathogenic microorganisms are resistant to the samples used in the study.

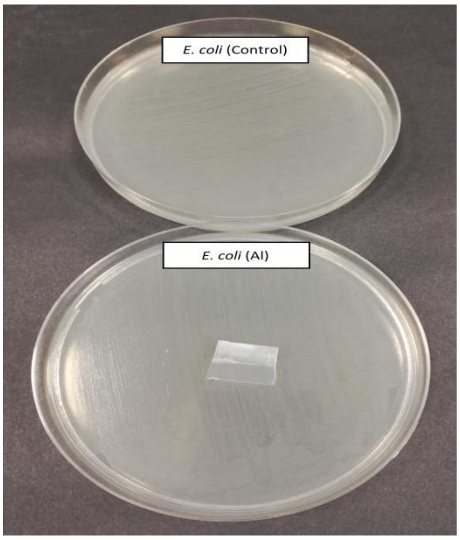

Figure 4.4 The antimicrobial activity of Al integrated into the glass surface

In El-Kattan *et al.* (2022) study, the antimicrobial activity of curcumin-doped Ag NPs (Cur-Ag NPs) at different concentrations (5, 10, 15, 20, 25 ppm) against pathogenic bacteria isolates (*Staphylococcus aureus* MSSA and MRSA, *Enterococcus faecalis, Pseudomonas aeruginosa, Klebsiella pneumoniae, Acinetobacter baumannii, Proteus vulgaris, Escherichia coli*) was determined and the zone diameters were found among 8.7-22.3 mm.

4.3 MIC and MLC/MBC Analysis

Minimum inhibition and minimum lethal concentration of power metals were carried out according to the method specified in antibacterial activity. MIC and MLC results of different concentrations of metals were given in Table 4.2.

Table 4.2 Minimum inhibition and minimum lethal concentration of power metals against *E. coli* and *S. aureus strains*

Pathogen Bacteria	**Minimum Inhibition Concentration (µg/mL)**		
	Al	Ni	Zn
E. coli	>5000	>5000	400
S. aureus	>5000	>5000	200
	Minimum Lethal Concentration (µg/mL)		
E. coli	>5000	>5000	500
S. aureus	>5000	>5000	250

As a result of the study, it was observed that the resistance of the pathogens to the metals used varies depending on the metal source and concentration. While the MIC value of *E. coli* bacteria varied between 400>5000 µg/mL, this value was determined as 200>5000 µg/mL in *S. aureus*. MLC values were designated as 500>5000 and 250>5000 µg/mL, respectively. Against *E. coli* bacteria at concentrations of 500 and 1000 µg/mL respectively. But Al, Ni metals could not inhibit bacterial growth and kill bacteria even at the highest concentration of 5000 µg/mL. It was found that Al, and Ni metals could not inhibit bacterial growth and kill bacteria at the highest concentration of 5000 µg/mL.

Souza *et al.* (2019) determinated the antibacterial activity of ZnO-NPs against important human foodborne pathogens (*Staphylococcus aureus, Salmonella* Typhimurium*, Bacillus cereus,* and *Pseudomonas aeruginosa*). The authors reported that the Minimum Inhibitory Concentration (MIC) and Minimum Bactericidal Concentration (MBC) were equal to 0.05 mg/mL and 0.5 mg/mL for *S. aureus* and *S.* Typhimurium, respectively. In another study, in which ZnO, TiO_2, and ZnO-TiO_2 nanoparticles were synthesized by sol-gel method using zinc acetate and titanium isopropoxide, the antifungal properties of nanopowders against *Aspergillus flavus* were investigated. MIC and MFC values for ZnO, and TiO_2, ZnO-TiO_2 against *A. flavus* were reported as 156, 78, 39 µg/mL, and 312, 156, 78 µg/mL, respectively (Ilkhechi *et al.* 2021).

4.4 Bacterial Adhesion and Survival Organism Counting

An adhesion test was performed to determine whether *E. coli* ATCC 35218 and *S. aureus* ATCC 25923 pathogenic microorganisms adhered to glass surfaces on which different metals were integrated. To prevent the growth of microorganisms during the adhesion experiments, the studies were carried out in PBS solution. The retention time was carried out as 4 hours. Antimicrobial activities against *E. coli* and *S. aureus* bacteria by survival organism counting method. The number of survival organisms after adhesion and adhesion rates were given in Table 4.3 and Table 4.4.

Table 4.3 Number of survival organisms after adhesion

Number of Survival Organisms (log_{10})				
Bacteria	Un-doped	Al	Ni	Control (bacteria)
E. coli	4.60	-	5.15	7.08
S. aureus	4.38	4.24	4.32	7.55

- not observed

Table 4.4 Bacterial adhesion on different metal surfaces and undoped surface

Bacterial Adhesion (%)		
Metal	*E. coli*	*S. aureus*
Un-doped	65.0	58.0
Al	-	56.2
Ni	72.7	57.2

In both bacteria, it was determined that as the metal additive percentage increased in the ZnO-Ni, Al added samples, there was a decrease in the adhesion percentages of the bacteria. While no bacterial adherence was observed in the Al-integrated glass sample treated with *E. coli*, 56.2 % adherence was observed in *S. aureus*. The highest and lowest adhesion rates were determined as Ni (72.7 %) and Al (0 %), Al (56.2 %) for *E. coli* and *S. aureus*, respectively.

Pathogenic microorganisms were kept on the metal sample integrated on the glass surface for 24 hours and viability counts were made at the end of the incubation period. No viability was observed in any of the glass samples. According to the results of the analysis, it was determined that *E. coli* and *S. aureus* bacteria were able to adhere to the metal samples integrated on the glass surface for 4 hours, but could not survive during the 24 hour waiting period. It is thought that alternative materials can be designed to inhibit or destroy the growth of pathogenic microorganisms with these metals because of there are no survival pathogenic microorganisms left on the surface and these materials have strong antibacterial and bactericidal effects. However, to reach a definite decision, it is recommended to conduct similar studies with other pathogenic microorganisms.

5. CONCLUSION

ZnO-based thin films are preferred in technological applications due to their many advantages. In this thesis study, undoped, Ni-doped and Al-doped ZnO thin films were produced on ITO substrate using the SILAR method. It was aimed to examine the properties of obtainde samples such as structural, superficial morphological, antibacterial, bacterial adhesion and survival organism count.

SEM Analysis;

When the SEM images of Al-doped ZnO are examined, the particles formed show an inhomogeneous structure in clusters. However, Al-doped ZnO nanoparticles appear to be scattered and clustered in voids on the surface. When the morphological structure of Ni doped ZnO thin film is examined, it is seen that it is coated on the ITO surface and synthesized homogeneously. It is also seen that there are some fractures due to surface tension.

EDS Analysis;

In the EDS analysis of the undoped ZnO sample, it is seen that the most dominant peak after the O peak belongs to the Zn peak. In addition, as can be seen from the EDS analysis, Na and Mg elements originate from impurity atoms.

In the EDS analysis of the Al-doped ZnO sample, it was observed that there was an Al peak, which is an additive element. In addition, the Mg peak is caused by impurity atoms.

In the EDS analysis of the Ni doped ZnO thin film, it was observed that the Ni peak, which is the doping element, was detected.

Antibacteria Analysis;

In other words, the pathogenic microorganisms are resistant to the study samples because the created samples did not exhibit antibacterial activity when the antibacterial activities were tested. Due to the fact that these materials exhibit potent antibacterial and antibacterial properties and that no pathogenic microorganisms are left to survive on the surface, it is believed that alternative materials can be created to hinder or eliminate the growth of pathogenic microorganisms.

In bacterial adhesion and survival organism count, the highest adhesion rate was observed in the Ni-doped thin film.

REFERENCES

Ahmad, R., Ahn, M. S. and Hahn, Y. B. 2017. ZnO nanorods array based field-effect transistor biosensor for phosphate detection. J. Colloid. Interf. Sci., 498: 292-297.

Akinwande, D., Brennan, C. J., Bunch, J. S., Egberts, P., Felts, J. R., Gao, H. and Zhu, Y. 2017. A review on mechanics and mechanical properties of 2D materials Graphene and beyond. Extreme Mechanics Letters, 13: 42-77.

Al-Hada, N. M., Kamari, H. M., Baqer, A. A., Shaari, A. H. and Saion, E. 2018. Thermal Calcination-Based Production of SnO_2 Nanopowder: An Analysis of SnO_2 Nanoparticle Characteristics and Antibacterial Activities. Nanomaterials, 8(4): 250.

Alim, S., Kafi, A. K. M., Rajan, J. and Yusoff, M. M. 2019. Application of polymerized multiporous nanofiber of SnO2 for designing a bienzyme glucose biosensor based on HRP/Gox. Int. J. Biol. Macromol., 123: 1028-1034.

Al-Mijalli, S. H., Mrabti, N. N., Ouassou, H., Sheikh, R. A., Abdallah, E. M., Assaggaf, H., Bakrim, S., Alshahrani, M. M., Al Awadh, A. A., Qasem, A., Attar, A., Lee, L. H., Bouyahya, A., Goh, K. W., Ming, L. C. and Hanae, H. N. 2022. Phytochemical variability, in vitro and in vivo biological ınvestigations, and ın silico antibacterial mechanisms of Mentha piperita essential oils collected from two different regions in Morocco. Foods, 11(21): 3466.

Alvarez, P. J., Chan, C. K., Elimelech, M., Halas, N. J. and Villagrán, D. 2018. Emerging opportunities for nanotechnology to enhance water security. Nature Nanotechnology, 13(8): 634-641.

Aydin, C. 2019. Synthesis of Pd: ZnO nanofibers and their optical characterization dependent on modified morphological properties. Journal of Alloys and Compounds, 777: 145-151.

Bhushan, B. 2017. Introduction to nanotechnology. In Springer handbook of nanotechnology, pp. 1-19, Berlin.

Borah, M. J., Devi, A., Borah, R. and Deka, D. 2019. Synthesis and application of Co doped ZnO as heterogeneous nanocatalyst for biodiesel production from non-edible oil. Renewable Energy, 133, 512-519.

Burla, M. C., Caliandro, R., Carrozzini, B., Cascarano, G. L., Cuocci, C., Giacovazzo, C. and Polidori, G. 2015. Crystal structure determination and refinement viaSIR2014. Journal of Applied Crystallography, 48(1): 306-309.

Cheng, Y., Chen, K. S., Meyer, N. L., Yuan, J., Hirst, L. S. and Chase, P. B. 2011. Functionalized SnO2 nanobelt field-effect transistor sensors for label-free detection of cardiac troponin. Biosens. Bioelectron. 26: 4538-4544.

Chua, P. H., Neoh, K. G., Kang, E. T. and Wang, W. 2008. Surface functionalization of titanium with hyaluronic acid/chitosan polyelectrolyte multilayers and RGD for promoting osteoblast functions and inhibiting bacterial adhesion. Biomaterials, 29(10): 1412-21.

Danial, E. N., Hjiri, M., Abdel-wahab, M. S. Alonizan, N. H., Mird, L. E. and Aida, M. S. 2020. Antibacterial activity of In-doped ZnO nanoparticles. Inorganic Chemistry Communications, 122, 108281.

de Francisco, E. V. and García-Estepa, R. M. 2018. Nanotechnology in the agrofood industry. Journal of Food Engineering, 238, 1-11.

Dong, S., Tong, M., Zhang, D. and Huang, T. 2017. The strategy of nitrite and immunoassay human IgG biosensors basedon ZnO@ZIF-8 and ionic liquid composite film. Sens. Actuat. B-Chem., 251: 650-657.

Dong, Y. and Zheng, J. 2014. A nonenzymatic L-cysteine sensor based on SnO_2-MWCNTs nanocomposites. J. Mol. Liq. 196: 280–284.

Duhan, J. S., Kumar, R., Kumar, N., Kaur, P., Nehra, K. and Duhan, S. 2017. Nanotechnology: The new perspective in precision agriculture. Biotechnology Reports, 15: 11-23.

Einollahzadeh, H., Fazeli, S. M. and Dariani, R. S. 2016. Studying the electronic and phononic structure of penta-graphane. Science and Technology of advanced MaTerialS, 17(1): 610-617.

El-Kattan, N., Emam, A. N., Mansour, A. S., Ibrahim, M. A., Abd El-Razik, A. B., Allam, K. A. M., Riad and N.Y., Ibrahim, S. A. 2022. Curcumin assisted green synthesis of silver and zinc oxide nanostructures and their antibacterial activity against some clinical pathogenic multi-drug resistant bacteria. RSC Advances, 12: 18022-18038.

Elmer, W. and White, J. C. 2018. The future of nanotechnology in plant pathology. Annual Review of Phytopathology, 56: 111-133.

Faria, A. M. and Mazon, T. 2019. Early diagnosis of zika infection using a ZnO nanostructures-based rapid electrochemical biosensor. Talanta, 203, 153-160.

Fiorani, A., Merino, J. P., Zanut, A., Criado, A. and Paolucci, F. 2019. Advanced carbon nanomaterials for electrochemiluminescent biosensor applications. Current Opinion in Electrochemistry, 16: 66-74.

Gehrke, I., Geiser, A. and Somborn-Schulz, A. 2015. Innovations in nanotechnology for water treatment. Nanotechnology, Science and Applications, 8: 1.

Grzybowski, B. A. and Huck, W. T. 2016. The nanotechnology of life-inspired systems. Nature Nanotechnology, 11(7): 585-592.

Gushurst, K. S., Nyman, J. and Boerrigter, S. X. 2019. The PO13 crystal structure of ROY. CrystEngComm, 21(9): 1363-1368.

Hanzl, P., Zetek, M., Bakša, T. and Kroupa, T. 2015. The influence of processing parameters on the mechanical properties of SLM parts. Procedia Engineering, 100: 1405-1413.

Hasnidawani, J. N., Azlina, H. N., Norita, H., Bonnia, N. N., Ratim, S. and Ali, E. S. 2016. Synthesis of ZnO nanostructures using sol-gel method. Procedia Chemistry, 19: 211-216.

Hornyak, G. L., Moore, J. J., Tibbals, H. F. and Dutta, J. 2018. Fundamentals of nanotechnology. CRC press. 13: 130-134.

Hulla, J. E., Sahu, S. C. and Hayes, A. W. 2015. Nanotechnology: History and future. Human & Experimental Toxicology, 34(12): 1318-1321.

Ibrahim Al Ahadeb, J. 2022. Impact of Cinnamomum verum against different Escherichia coli strains isolated from drinking water sources of rural areas in Riyadh, Saudi Arabia. Journal of King Saud University Science, 34(2): 101742.

Ilkhechi, N. N., Mozammel, M. and Khosroushahi, A. Y. 2021. Antifungal effects of ZnO, TiO2 and ZnO-TiO2 nanostructures on Aspergillus flavus. Pesticide Biochemistry and Physiology, 176: 104869.

Karthik, K. V., Raghu, A. V., Reddy, K. R., Ravishankar, R., Sangeeta, M., Shetti, N. P. and Reddy, C. V. 2022. Green synthesis of Cu-doped ZnO nanoparticles and its application for the photocatalytic degradation of hazardous organic pollutants. Chemosphere, 28(7): 132081.

Laguna-Marco, M. A., Kayser, P., Alonso, J. A., Martínez-Lope, M. J., Van Veenendaal, M., Choi, Y. and Haskel, D. 2015. Electronic structure, local magnetism, and spin-orbit effects of Ir IV-, Ir V-, and Ir VI-based compounds. Physical Review B, 91(21): 214433.

Lavanya, N., Radhakrishnan, S. and Sekar, C. 2012. Fabrication of hydrogen peroxide biosensor based on Ni doped SnO2 nanoparticles. Biosens. Bioelectron., 36: 41-47.

Lei, Y., Yan, X., Zhao, J., Liu, X., Song, Y. and Luo, N. 2011. Improved glucose electrochemical biosensor by appropriate immobilization of nano-ZnO, Colloid. Surface. B., 82: 168-172.

Li, L., Huang, J., Wang, Y., Zhang, H., Liu, Y. and Li, J. 2010. An excellent enzyme biosensor based on Sbdoped SnO2 nanowires. Biosens. Bioelectron. 25: 2436-2441.

Lowry, G. V., Avellan, A. and Gilbertson, L. M. 2019. Opportunities and challenges for nanotechnology in the agri-tech revolution. Nature Nanotechnology, 14(6): 517-522.

Ma, Q., Guo, R., Zhao, Z., Lin, Z. and He, K. 2015. Mechanical properties of concrete at high temperature A review. Construction and Building Materials, 9(3): 371-383.

Manjunatha, S. B., Biradar, D. P. and Aladakatti, Y. R. 2016. Nanotechnology and its applications in agriculture: A review. Journal of Agricultural Food, 291: 1-13.

Manoj, A. M., Viannie, L. R., Subramaniam, C. K., Raj, N. A. N. and Manivasagam, G. 2021. Single-step hydrothermal synthesis of nitrogen-doped ZnO nanostructures and an insight into its electrochemical properties. Journal of Materials Research, 36(2): 350-360.

Nasrollahzadeh, M., Sajjadi, M., Sajadi, S. M. and Issaabadi, Z. 2019. Green nanotechnology. In Interface Science and Technology, 28: 145-198.

Nayak, C. B., Taware, P. P., Jagadale, U. T., Jadhav, N. A. and Morkhade, S. G. 2022. Effect of SiO2 and ZnO nano-composites on mechanical and chemical properties of modified concrete. Iranian Journal of Science and Technology, Transactions of Civil Engineering, 46(2): 1237-1247.

Nikalje, A. P. 2015. Nanotechnology and its applications in medicine. Med. Chem., 52: 081-089.

Peiner, C., Löcken, H., Reinsch, L. and Gries, T. 2022. 3D Knitted Preforms Using Large Circular Weft Knitting Machines. Applied Composite Materials, 29: 273-288.

Pramanik, P., Krishnan, P., Maity, A., Mridha, N., Mukherjee, A. and Rai, V. 2020. Application of nanotechnology in agriculture. In Environmental Nanotechnology, 4: 317-348.

Prasad, R., Bhattacharyya, A. and Nguyen, Q. D. 2017. Nanotechnology in sustainable agriculture: recent developments, challenges, and perspectives. Frontiers in Microbiology, 8: 1014.

Raizada, P., Sudhaik, A. and Singh, P. 2019. Photocatalytic water decontamination using graphene and ZnO coupled photocatalysts: a review. Materials Science for Energy Technologies, 23: 509-525.

Ramon-Marquez, T., Medina-Castillo, A. L., Fernandez-Gutierrez, A. and Fernandez-Sanchez, J. F. (2018). Evaluation of two sterically directed attachments of biomolecules on a coaxial nanofibre membrane to improve the development of optical biosensors. Talanta., 187: 83-90.

Ranjith, K. S. and Kumar, R. R. 2017. Regeneration of an efficient, solar active hierarchical ZnO flower photocatalyst for repeatable usage: controlled desorption of poisoned species from active catalytic sites. RSC Advances, 79: 4983-4992.

Reinheimer, J., Demkow, M. and Condioti M. 1990. Inhibition of coliform bacteria by lactic cultures. Australian Journal of Dairy Technology, 45(1): 5-9.

Römelt, C., Song, J., Tarrago, M., Rees, J. A., van Gastel, M., Weyhermüller, T. and Ye, S. 2017. Electronic structure of a formal iron 0 porphyrin complex relevant to CO_2 reduction. Inorganic Chemistry, 56(8): 4745-4750.

Rotzler, S., Malzahn, J., Werft, L., von Krshiwoblozki, M. and Eppinger, E. 2022. Influence of Knitting and Material Parameters on the Quality and Reliability of Knitted Conductor Tracks. Textiles, 2: 524-545.

Sadhukhan, P., Kundu, M., Rana, S., Kumar, R., Das, J. and Sil, P. C. 2019. Microwave induced synthesis of ZnO nanorods and their efficacy as a drug carrier with profound anticancer and antibacterial properties. Toxicology Reports, 6: 176-185.

Sanzari, I., Leone, A., & Ambrosone, A. 2019. Nanotechnology in plant science: to make a long story short. Frontiers in Bioengineering and Biotechnology, 7: 120.

Saranya, M., Ramachandran, R. and Wang, F. 2016. Graphene-zinc oxide G-ZnO nanocomposite for electrochemical supercapacitor applications. Journal of Science: Advanced Materials and Devices, 1(4): 454-460.

Senthil Kumar, B., & Ramachandran, T. 2018. Influence of knitting process parameters on the thermal comfort properties of eri silk knitted fabrics. Fibres & Textiles in Eastern Europe, 13: 13-134.

Sheldrick, G. M. 2015. SHELXT-Integrated space-group and crystal-structure determination. Acta Crystallographica Section A: Foundations and Advances, 71(1): 3-8.

Shohany, B. G. and Zak, A. K. 2020. Doped ZnO nanostructures with selected elements-Structural, morphology and optical properties: A review. Ceramics International, 46(5): 5507-5520.

Silvestre, J., Silvestre, N. and De Brito, J. 2016. Review on concrete nanotechnology. European Journal of Environmental and Civil Engineering, 20(4): 455-485.

Singh, S., Li, C., Panzer, F., Narasimhan, K. L., Graeser, A., Gujar, T. P. and Kabra, D. 2016. Effect of thermal and structural disorder on the electronic structure of hybrid perovskite semiconductor $CH_3NH_3PbI_3$. The journal of Physical Chemistry Letters, 71(5): 3014-3021.

Singh, T., Shukla, S., Kumar, P., Wahla, V., Bajpai, V. K. and Rather, I. A. 2017. Application of nanotechnology in food science: perception and overview. Frontiers in Microbiology, 8: 1501.

Sinha, M., Mahapatra, R., Mondal, B., Maruyama, T. and Ghosh, R. 2016. Ultrafast and reversible gas-sensing properties of ZnO nanowire arrays grown by hydrothermal technique. The Journal of Physical Chemistry C, 120(5): 3019-3025.

Souza, R. C., Haberbeck, L. U., Riella, H. G., Ribeiro, D. H. B. and Carciofi, B. A. M. 2019. Antibacterial Activity of Zinc Oxide Nanoparticles Synthesized by Solochemical Process. Brazilian Journal of Chemical Engineering, 36(2): 885-893.

Suntako, R. 2015. Effect of zinc oxide nanoparticles synthesized by a precipitation method on mechanical and morphological properties of the CR foam. Bulletin of Materials Science, 38(4): 1033-1038.

Tiwari, V., Matutes, Y. A., Gardiner, A. T., Jansen, T. L., Cogdell, R. J. and Ogilvie, J. P. 2018. Spatially-resolved fluorescence-detected two-dimensional electronic spectroscopy probes varying excitonic structure in photosynthetic bacteria. Nature Communications, 9(1): 1-10.

Uikey, Prateek, and Kirti Vishwakarma. "Review of zinc oxide ZnO nanoparticles applications and properties." International Journal of Emerging Technology in Computer Science & Electronics 21.2 2016: 239-42.

Usman, M., Farooq, M., Wakeel, A., Nawaz, A., Cheema, S. A., ur Rehman, H., & Sanaullah, M. 2020. Nanotechnology in agriculture: Current status, challenges and future opportunities. Science of the Total Environment, 721: 137778.

Vartiainen, J., Rättö, M., Tapper, U., Paulussen, S. and Hurme, E. 2005. Surface modification of atmospheric plasma activated BOPP by immobilizing chitosan. Polymer Bulletin, 54: 343-352.

Verma, S. K., Panda, P. K., Jha, E., Suar, M. and Parashar, S. K. S. 2017. Altered physiochemical properties in industrially synthesized ZnO nanoparticles regulate oxidative stress; induce in vivo cytotoxicity in embryonic zebrafish by apoptosis. Scientific Reports, 7(1): 1-16.

Wang, P., Lombi, E., Zhao, F. J. and Kopittke, P. M. 2016. Nanotechnology: a new opportunity in plant sciences. Trends in Plant Science, 21(8): 699-712.

Wang, Q., Zhao, Y., Yang, Q., Du, D. and Lin, Y. 2019. Amperometric sarcosine biosensor with strong anti-interference capabilities based on mesoporous organic-inorganic hybrid materials. Biosens. Bioelectron. 141: 111431.

Wang, Y., Fan, D., Zhao, G., Feng, J., Wei, D. and Zhang, N. 2018. Ultrasensitive photoelectrochemical immunosensor for the detection of amyloid β-protein based on SnO2/SnS2/Ag2S nanocomposites. Biosens. Bioelectron. 120: 1-7.

Wang, Z., Bockstaller, M. R. and Matyjaszewski, K. 2021. Synthesis and applications of ZnO/polymer nanohybrids. ACS Materials Letters, 3(5): 599-621.

Weldegebrieal, G. K. 2020. Synthesis method, antibacterial and photocatalytic activity of ZnO nanoparticles for azo dyes in wastewater treatment: A review. Inorganic Chemistry Communications, 120: 108140.

Yetisen, A. K., Qu, H., Manbachi, A., Butt, H., Dokmeci, M. R., Hinestroza, J. P. and Yun, S. H. 2016. Nanotechnology in textiles. ACS Nano, 10(3): 3042-3068.

Yibar, M. F., Ogut, H., Cingu, N., Cetin, S., Yatikci, T. K. and Yildirim, K. 2022. Influence of some knitting and finishing parameters on the snag resistance of polyethylene terephthalate PET knit fabric. Textile Research Journal, 9(2): 801-809.

Yilmaz, Y. Y., Yalcinkaya, E. E., Demirkol, D. O. and Timur, S. 2020. 4-aminothiophenol-intercalated montmorillonite: Organic-inorganic hybrid material as an immobilization support for biosensors. Sensors and Actuators B: Chemical. 307:127665.

Yin, M.-J., Gu, B., An, Q.-F., Yang, C. and Yong, K. T. 2018. Recent development of fiber-optic chemical sensors and biosensors: Mechanisms, materials, micro/nano-fabrications and applications. Coordination Chemistry Reviews, 376, 348-392.

Yuea, H. Y., Zhanga, H. J., Huanga, S., Lua, X. X., Gaoa, X., Songa, S. S. 2020. Highly sensitive and selective dopamine biosensor using Au nanoparticles-ZnO nanocone arrays/graphene foam electrode. Materials Science and Engineering, C 108: 110490.

Zagorac, D., Müller, H., Ruehl, S., Zagorac, J. and Rehme, S. 2019. Recent developments in the Inorganic Crystal Structure Database: theoretical crystal structure data and related features. Journal of Applied Crystallography, 52(5): 918-925.

Zhang, X., Li, W., Zhou, Y., Chai, Y. and Yuan, R. 2019. An ultrasensitive electrochemiluminescence biosensor for MicroRNA detection based on luminol-functionalized Au NPs@ZnO nanomaterials as signal probe and dissolved O2 as coreactant. Biosensors and Bioelectronics, 135: 8-13.

Zhang, Y., Li, M., Gao, X., Chen, Y. and Liu, T. 2019. Nanotechnology in cancer diagnosis: progress, challenges and opportunities. Journal of Hematology and Oncology, 12(1): 1-13.

Zhou, Q., Yang, L., Wang, G. and Yang, Y. 2013. Acetylcholinesterase biosensor based on SnO2 nanoparticles–carboxylic graphene-nafion modified electrode for detection of pesticides. Biosensors and Bioelectronics, 49: 25-31.

Zong, X. and Zhu, R. 2018. ZnO nanorod-based FET biosensor for continuous glucose monitoring. Sensors and Actuators B: Chemical, 255, 2448-2453.